Journal of Geosciences and Geomatics, 2022, Vol. 10, No. 2, 99-111
Available online at http://pubs.sciepub.com/jgg/10/2/4
Published by Science and Education Publishing
DOI:10.12691/jgg-10-2-4

Migration and Retention of Uranium in the Weathering Blanket Developed on Uraniferous Syenite in Ngombas Southern Cameroon

Joel Simon Mbai[1,*], Akumbom Vishiti[1], Bravo Martin Mbang Bonda[1], Gilbert François NGON NGON[2], Elie Constantin Bayiga[2], Martine Gérard[3], Jacques Etamè[1,2]

[1]The University Institute of Technology, University of Douala, P.O Box 8698, Douala, Cameroon
[2]University of Douala, Faculty of Sciences, P.O Box 24157, Douala, Cameroon
[3]Sorbonne Universités CNRS UMR 7590, MNHN, IRD, Institut de Minéralogie,
de Physique des Matériaux, et de Cosmochimie (IMPMC), 4 Place Jussieu, Paris F-75005, France
*Corresponding author: mbai_s@yahoo.fr

Received April 09, 2022; Revised May 14, 2022; Accepted May 23, 2022

Abstract The lolodorf syenite axis is known for its radiometric indices. In the Ngombas area the migration and retention of uranium in the regolith developed on syenite is studied using a combination of mineralogy and geochemistry in a bid to understand the processes involved in the dissolution and redistribution of uranium in the secondary environment. A trench dug in the area shows three horizons from the bottom to the top. They include the saprolite, B and Ah horizons. Petrographic and XRD investigations of the syenites reveals minerals such as plagioclase, potassic feldspar, amphibole, pyroxene, biotite, quartz, hematite, zircon coupled with uraninite, U-monazite. The regolith developed on the syenite shows relics of plagioclase, amphibole, quartz, hematite, goethite, chlorite, vermiculite, kaolinite. This is associated with U-bearing minerals such as uranothorite, U-monazite, U-zircon, U-florencite and U-rhadophane. The chemical alteration index (CIA), and gain and loss diagrams indicate that the horizons are more weathered from the top to the bottom. The presence of uranium bearing phases such as uranothorite indicates that U-minerals were dissolved, migrated and sorbed on thorite. The occurrences of U-florencite and U-rhabdophane in the weathering blanket indicate that uranyl is stabilized by phosphate minerals. Under oxidizing conditions the stability of hexavalent uranium is favored by the presence of clay minerals and Fe/Mn-oxyhydroxides. Thus, the migration of uranium in Ngombas is sequestrated by clay blended on Fe-oxides through the process of sorption. The U-bearing phases in the regolith that survived weathering include monazite and zircon. The presence of accessories minerals (U-zircon, U-monazite), sorption of uranium by phosphates, by Fe/Mn-oxyhydroxides, and clays minerals play important roles to reduce the U migration in environmental impact of Ngombas region.

Keywords: *uranium, migration, weathering, uraniferous syenite, tropics, Cameroon*

Cite This Article: Joel Simon Mbai, Akumbom Vishiti, Bravo Martin Mbang Bonda, Gilbert François NGON NGON, Elie Constantin Bayiga, Martine Gérard, and Jacques Etamè, "Migration and Retention of Uranium in the Weathering Blanket Developed on Uraniferous Syenite in Ngombas Southern Cameroon." *Journal of Geosciences and Geomatics*, vol. 10, no. 2 (2022): 99-111. doi: 10.12691/jgg-10-2-4.

1. Introduction

The weathering blanket in the southern region of Cameroon proceeds from the weathering of many rocks types and, characterizes a humid tropical climate zone [1,2,3,4,5]. Generally, weathered products also called laterite, includes (from bottom to top): coarse saprolite, fine saprolite, nodular and loose clay horizon [6,7]. These components of weathered materials are precursory of soil formation [6]. Increasing weathering breaks down the parent rock which leads to the formation of secondary minerals [8] and enables the mobility of chemical elements in the weathering blanket [9,10]. According to [8,10,11,12,13,14] during weathering, the primary minerals are continually transformed to clay minerals (kaolinite, smectite, vermiculite etc..) and/or Fe-oxyhydroxydes, accompanied by the migration and redistribution of elements. The behavior of chemical element during weathering is controlled by parameters suc as pH, redox conditions, sorption (adsorption/desorption), compatibility/incompatibility and the presence of organic matter [13,14,15].

The migration of uranium depends on the redox condition in the parent rock. It has been shown that the climate transforms the primary uranium (U^{+4}) mineral (uraninite, coffinite, brannerite) in rock to uranyl ions UO_2 (U^{+6}) in the soils or waste rocks [16,17,18,19,20]. The mobility of uranyl ions (U^{6+}) in the weathered blanket is inhibited or naturally attenuated by the formation of complexes controlled by sorption process, that influences speciation of uranium in oxidizing conditions [21,22].

According to [23], the uranyl ions do not migrate in acidic conditions but when stabilized in soil in weak acidic to near neutral pH ranges [20]. Secondary U-mineral phases include autunite, schoepite, jarosite. Despite the occurrence of several secondary U-mineral phases, phosphates are the main stable form of uranium in weathering environment [20,22]. In the soil, clay minerals (kaolinite, montmollorinite, illite, clinochlore) and iron oxyhydroxides (hematite, goethite, ferrihydrite) sequestrate uranyl ion (U (VI)) by sorption and/or co-precipitation [17,18,19,20,24,25,26].

Studies of uranium migration in soils of humid equatorial area are rare. Nevertheless, the weathering of the rocks [1,3,8,27] and the geological context of uranium mineralization in tropical regions [28-38] have been discussed in detail.

In Cameroon, the research for uranium began around the 1970's [39]. Results revealed radiometrics anomalies in granites and nephelinitic syenites. The occurrence of uranium in granite is reported in Ekomedion [36,37], Lolodorf and Kitongo [35]. Radiometric anomalies have been identified along the Lokoundje River Basin which dissects through radioactive syenite sources [40,41,42]. Recent research reveals that alpha emitting radionucleides in Melondo and Ngombas attribute radiometric anomalies to the presence of Th, U, Po, Ra in soils and fern [42].

In the Southern Cameroon, studies on uraniferous syenite have focused on the description of the weathering profile, the behavior of Ce, REE and Th [43,44], and the genesis of soils [8]. In this study we evaluate the petrology, mineralogy and geochemistry of uraniferous syenite as well as the weathering blanket developed on them in a bid to understand the processes involved in the migration of U from the primary rock into the secondary environment in Ngombas Southern Cameroon.

2. Geological Setting

The Nyong complex of Pan-African age in the southern part of Cameroon belongs to the West Central African Belt (WCAB). It was set in place by the remobilization of the Western part of the Congo craton during the Central Eburnean orogeny (2400-1800Ma), with slight shear of juvenile material from the collision between the Congo and San Francisco craton [45,46,47,48,49]. Two tectonics phases have been recorded in the Ntem complex. They include the Eburnean and Pan-African reactivation (Figure 1A) [40,47,48,49]. The Nyong complex is characterized by amphibolite, quartzite, metagranitoide, TTG, anorthosite, metagabbro, charnokite, gneiss bearing magnetite, alkaline metasyenites and BIFs are the main petrographic features [12,40,49,50], with soils that are generally to the ferralitic and hydromorphic soil [8].

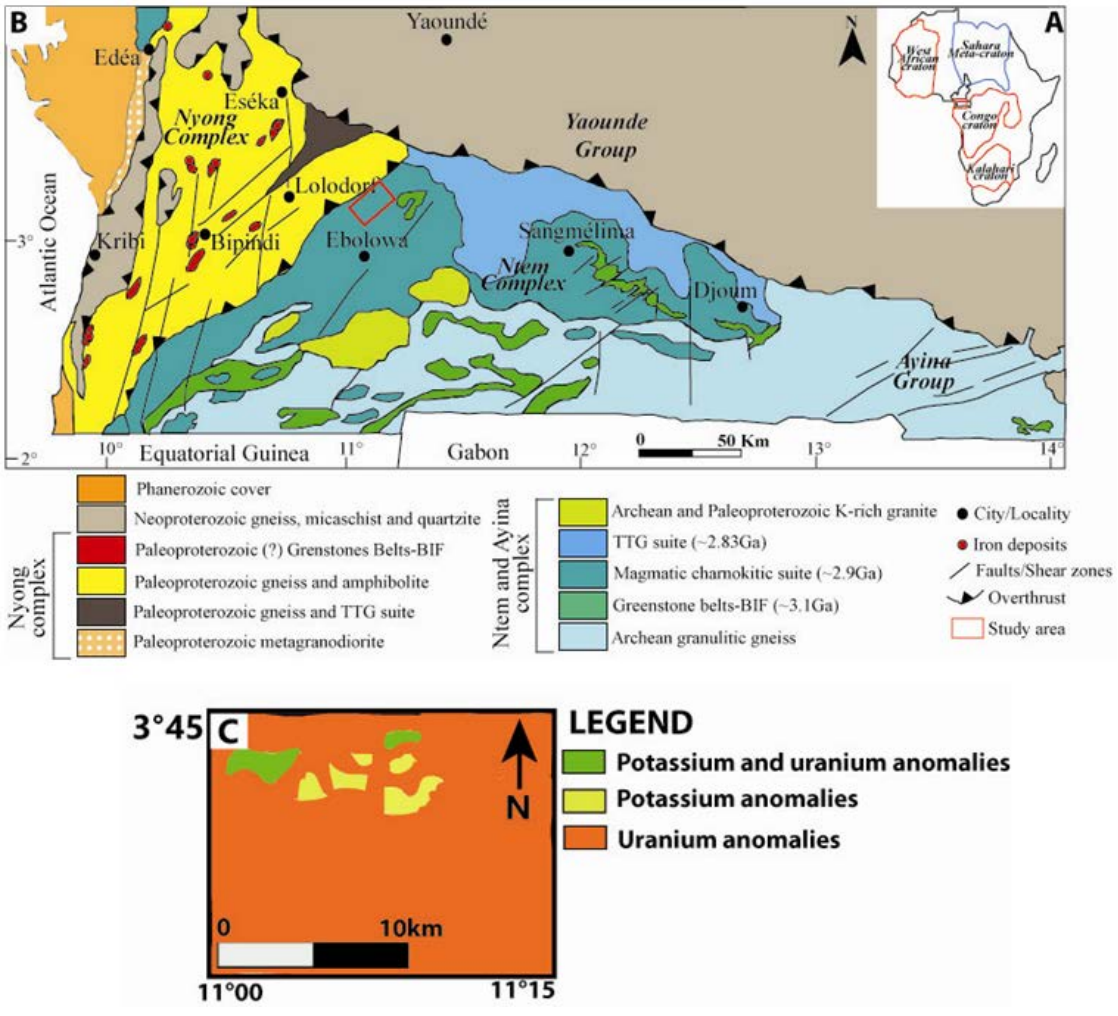

Figure 1. Location and geological map of southern Cameroon. A: location map of Cameroon. B: Geological map of southern Cameroon. C: Radiometric anomaly of Ngombas (modified after [40,41])

Ngombas is located in the Southern part of Cameroon (3°28 N-10°90 E and 3°21N -10°58 E (Figure 1B). The climate is subequatorial with four seasons marked by two rainy seasons and two dry seasons. The average annual rainfall and temperatures are respectively 1500 mm to 2000 mm and 24°C [51]. The dense rainforest vegetation is affected by anthropic activities [52]. The morphology is characterized by variable relief reaching 500 to 700 m. The relief is dominated by peneplanes, hills dissected by U and V shape valleys.

3. Material and Methods

3.1. Site Selection and Samples Collection

During the search of uranium indices in the southern part of Cameroon, a uranium anomaly was identified along the Lolodorf syenitic axis http://www.megauranium.com /main/?kitongololodorf. In order to evaluate the behavior of U in the regolith developed on the bedrock a trench was dug to the bedrock to expose systematically the weathering blanket. The horizons identified were characterized base on their color, texture, structure and mineralogy. Nine samples (rock and soil) were collected from the trenches using the channel chip sampling method. Samples collected were bagged and transported to the University of Douala for further separation and preparation for geochemical analysis.

3.2. Analytical Procedures

A section of each sample was used to prepare polished thin sections (rock, saprolite and impregnated horizon B) at the Institut de Recherche pour le Développement (IRD), Bondy Research Center France. The thin sections were observed under the Nikon Eclipse LV100 optical microscope for their petrographic properties. They were then mounted on a Zeiss ULTRA55 microscope in order to determine the mineral phases present.

SEM images using backscattered electron mode (BSE) were recorded at 5, 20 and 25 keV on a Zeiss Supra VP in the ECCE TERRA, at Observatoire des Sciences de I'Univers, Sorbonne University-INSU. The chemical compositions of the U-bearing mineral phases were determined on a CAMECASX-FIVE equipped with five WDS and one EDS detector at CAMPARIS ECCE TERRA, Sorbonne University. The spatial resolution was set at 1 μm^2. WDS microprobe characterization was achieved for oxides of Al, Si, P, K, Ca, Ti, V, Mn, Fe, Y, Ce, Pb, Th, U, Na and Mg.

Major mineral phases were analyzed by powder XRD. Prior to that the samples were crushed in a marble crusher and pulverized using an agate motar and pestle. The 30 µm size fraction obtained was mounted with a random orientation in aluminium rotating sample holder and analyzed with an X'pert Pro Panalytical diffractometer using an X'Celerator detector and Cu Kα (1.54 Å) or Co Kα (1.79 Å) monochromatic sources at 40 kV and 40 mA. Instrumental conditions were as follows 40 kV, 40 mA, goniometerscan from 3^o to 70^o 2θ with count time of 10800s every 0.016^o. In order to identify the clay mineral fraction, 10 g of bulk samples were mixed with deionized water and ultrasound for 10 minutes in order to separate agglomerated minerals. After 1800s, the float was deposited on a glass-disk holder and air dried to obtain the fag fraction. The oriented samples were glycolated and heated (500°C for 3h) and then scanned from 3° to 15° 2θ with a counting time of 1800s every 0.0167°. An interactive software ESPRIT Bruker was used to identify the main mineral phases present. Identification was based on multiple peak matches using the mineral data base provided by the software.

The chemical compositions of the samples were determined at the ALS Global Chemex Laboratory in Petroria, South Africa. Loss on ignition was achieved by heating the powder samples at 105°C under nitrogen to eliminate water, and at 1000°C under oxygen to extract volatile components. Major and trace elements were analyzed using a combination of inductively coupled plasma-atomic emissions (ICP-AES) and inductively coupled plasma-mass spectrometry (ICP-MS) respectively. Prior to analysis, samples were digested in HF, HNO3, and HCLO4 acids. The samples were analyzed at a temperature of 200°C within pressure-tight Teflon cups, and then the dissolved solution was measured on a Perkin Elmer Elan 9000 instrument. Standards and duplicates were analyzed for quality control. The detection limits varies from 0.01 to 0.05 for the major elements and from 0.1 to 0.5 for the trace elements. The geochemical trends during weathering were determined as a function of the degree of chemical weathering using the chemical index of alteration [53]. The element dispersion between the basement rock and the regolith were then computed using the mass balance method of with TiO_2 as the least mobile element of choice.

4. Results

4.1. Petrology of Syenite and the Weathering Materials

4.1.1. Syenite

Syenite is coarse-grained and gray to greenish in color (Figure 2). It is heterogranular and is composed predominantly of plagioclase, potassic feldspar, amphibole, biotite, quartz, hematite, zircon, apatite, epidote and oxides (Figure 3 and Figure 4). Syenite bears uranium mineral such as uraninite, U-monazite and U-zircon (Figure 5a and Figure 5b). Clay minerals identified include kaolinite and chlorite (Figure 4a). Plagioclase is common in the syenites. It is subangular and in some cases occurs as inclusions in zircon (Figure 3a). Biotite is elongated in shape (Figure 3a). Amphibole and quartz are euhedral (Figure 3a and Figure 3b) and occurs as disseminations in the groundmass. Zircon occurs as inclusion in uraninite. U bearing phases in the syenite occurs in the form of uraninite, U-monazite and U-zircon. U-monazite and U-zircon are associated with apatite and plagioclase respectively (Figure 5a and Figure 5b).

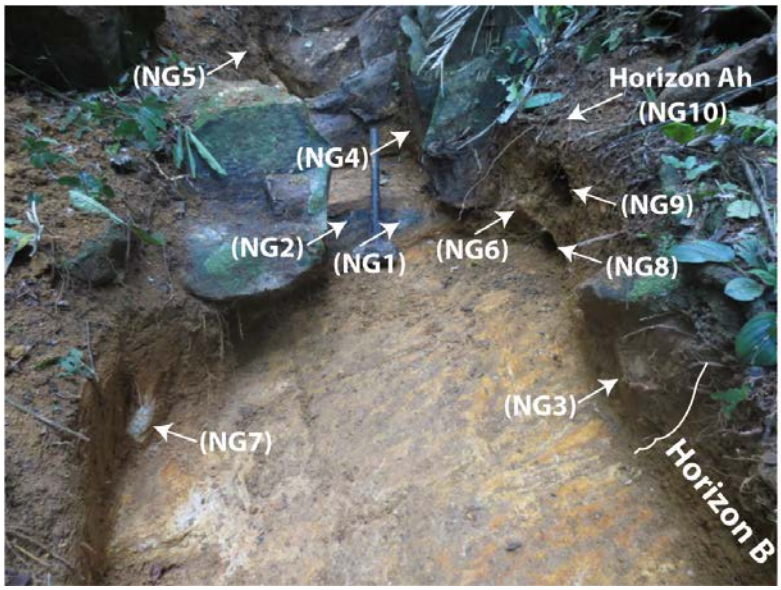

Figure 2. Trench opened in the Ngombas area indicating the location of the samples used in this study

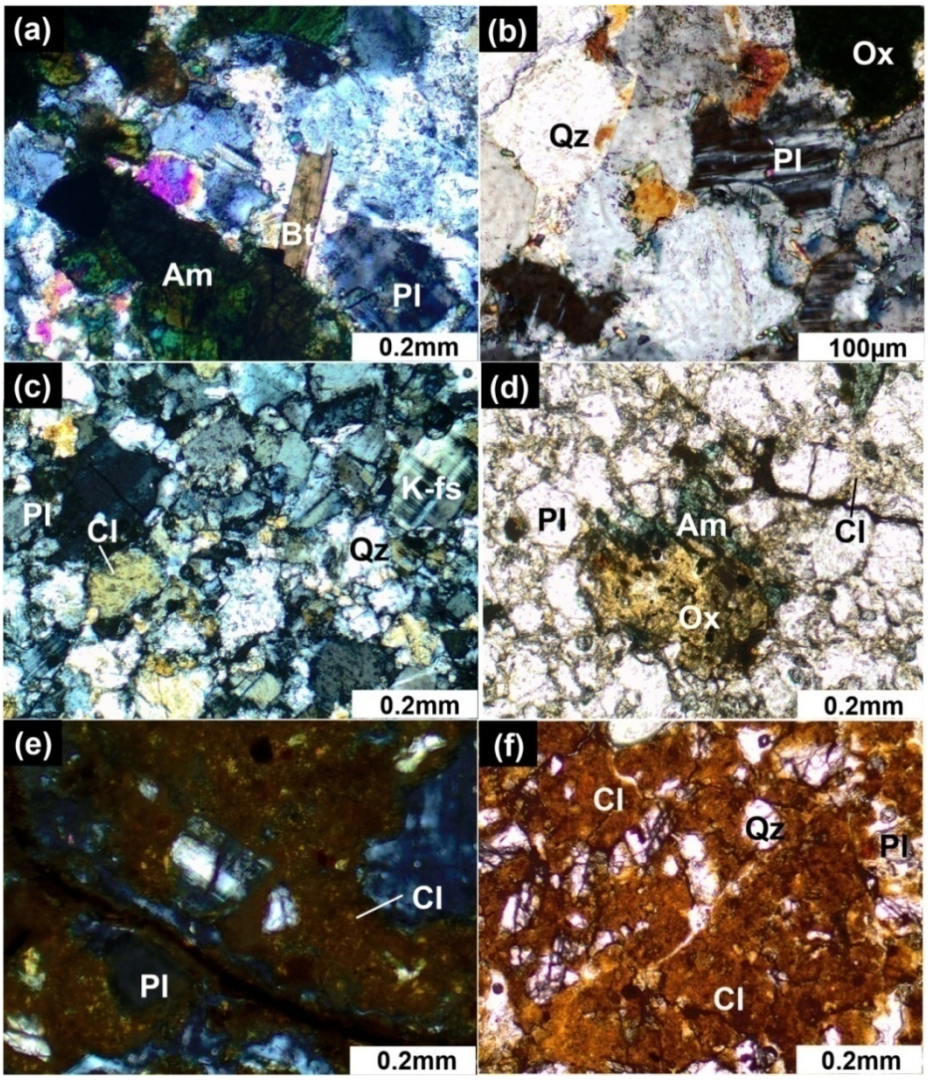

Figure 3. Representative photomicrographs of syenite and the weathering blanket taken under plane polarized light and crossed polars. (a) syenite showing microcrystals of plagioclase, biotite and amphibole. (b) Opaque minerals surrounding the lamelar crystal of plagioclase and quartz. (c) Saprolite horizon showing quartz, plagioclase and clay (d): Saprolite horizon showing opaque mineral mainly oxides, amphibole, plagioclase and clay. (e) Horizon B showing crystals of plagioclase in a clayey matrix. (f) Horizon Ah reveals clayey matrix trapping plagioclase and quartz Abbreviations translate as follows: Pl=plagioclase, Bt= biotite, Am=amphibole, Qz=quartz, Hm=hematite, Ox=oxides, Cl=clay mineral, K-Fs=feldspar , Zr= zircon

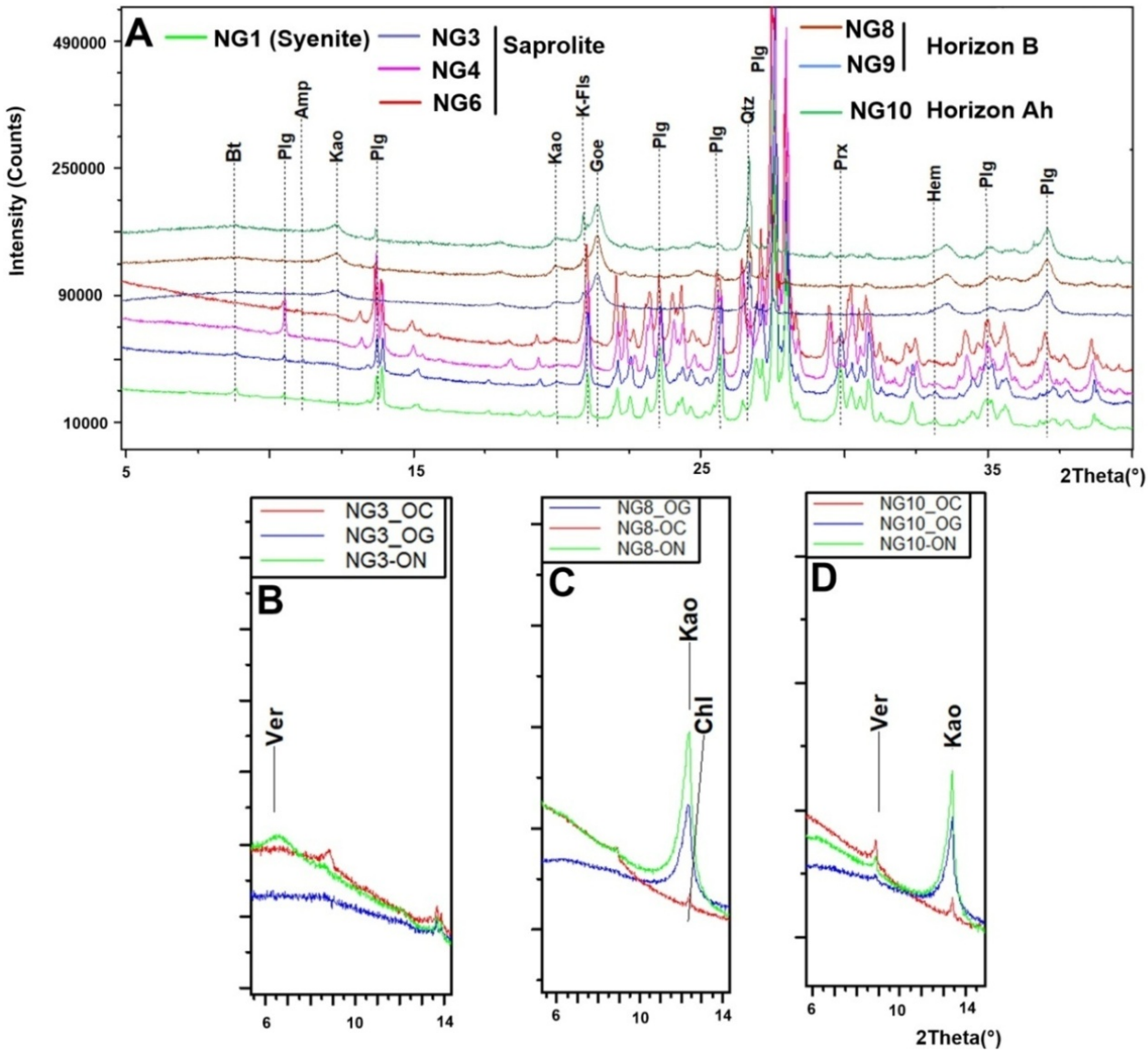

Figure 4. XRD patterns on bulk samples of the basement rock and their weathering blankets showing primary and secondary mineral phases. (A): Mineralogical composition of the syenite and its weathering blanket. (B): Mineralogical composition of the fine fraction of saprolite. (C) Mineralogical composition of the fine fraction of horizon B. (D) Mineralogical composition of the fine fraction of horizon Ah. Abbreviations translate as follows, Chl: chlorite, Sm: smectite, Ver: vermiculite, Kao: kaolinite, Bt: biotite, Amp: amphibole, Kfs: K-feldspar, Goe: goethite, Plg: plagioclase, Qtz: quartz, Prx: pyroxene, Hem: hematite, Prx : pyroxene

4.1.2. Weathering Materials

The weathering materials that developed on the syenite reveal three horizons from the bottom to the top: saprolite, B horizon and the Ah horizon. The saprolite is red in color and reveals the structure of the bedrock (Figure 2). The saprolite shows desiccation with micro-cracks sometimes filled with clay and fine gravel. It has a thickness of 25 cm. It reveals relics of plagioclase, potassic feldspar quartz and clay minerals (Figure 3c and Figure 5b). Relics of amphibole are associated with oxides. Uranium-bearing phases identified here include uranothorite, U-florencite and U-monazite (Figure 5c, Figure 5d and Figure 5e). While uranothorite is associated with chlorite (Figure 5c). U-florencite occurs as inclusion in apatite which one is intersected by U-monazite (Figure 5e).

The B horizon preserves only relics of the parent rock and some roots. It is clayey and shows a clotty structure. It is yellowish in color and has a thickness from 55.5 cm and slight porose (Figure 2). Relics of plagioclase and quartz occur as inclusions in clay minerals (Figure 3e). Clay minerals identified here include vermiculites, chlorite and kaolinite (Figure 4c). Uranium phases identified are uranothorite, U-rabdophane, U-zircon and uranium in kaolinite (Figure 5f).

The Ah horizon is 15 cm thick. It is clayey and varies in color from gray to brownish yellow (Figure 2). It is porous contains humus. The weathering materials show relics of amphibole, plagioclase, potassic feldspar quartz and clay minerals (Figure 3f) such as vermiculites, chlorite and kaolinite (Figure 4d). The iron oxides minerals identified here include hematite and goethite blended in clay (Figure 4a).

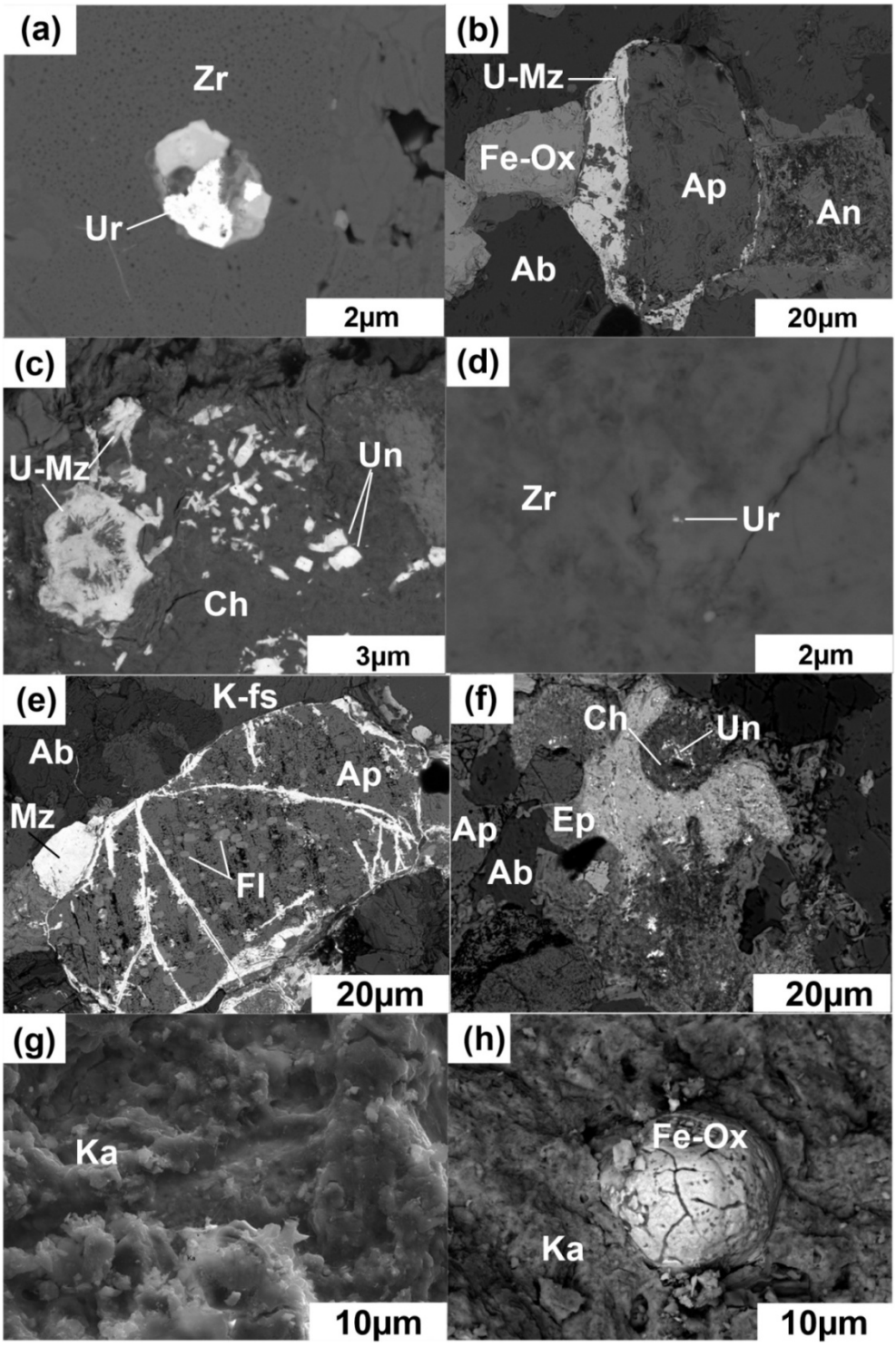

Figure 5. Representative SEM images and EDS pattern from the syenite rock (a-b) and horizons (c-e : saprolite, f : horizon B, g-h horizon Ah). (a) syenite showing inclusion of uraninite in zircon. (b) U-monazite surrounding apatite in syenite. (c) Uranothorite and U-monazite on chlorite (d) microcrystal of uraninite in zircon inclusion. (e) Apatite trapping subangular U-florencite minerals. (f) Uranothorite on chlorite mineral. (g) SEM image of kaolinite. (h) SEM image of iron oxide trapped in kaolinite Abbreviations translate as follows, Zr : zircon, Ch : chlorite, Ab : albite, U-florencite, Ka : kaolinite, Ep : epidote, An : allanite, Ap: apatite, Ver: vermiculite, Ur: uraninite, U-Mz: U-monazite

4.2. Microchemistry of Uranium Bearing Phases

Electron microprobe analysis on U-bearing phases (Table 1) such as uraninite, U-zircon, U-monazite uranothorite, U-florencite, U-rabdophane and U-kaolinite in syenite and the weathering material shows a variation in the content of UO_2. In the syenite, uraninite is the main uranium bearing phase with a concentration of 80.82 wt% UO_2. The concentration of UO_2 in U-zircon varies from 0.11 to 0.74 wt%. U phases identified in the saprolite show UO_2 content that varies between 0.28 and 1.94 wt% in U-monazite, 0.28 wt% in U-florencite and 26.37 wt% in the uranothorite. The B horizon reveals 24.37 wt% UO_2 in uranothorite, 0.4 wt% in zircon, 0.21 wt% in rabdophane and from 0.14 to 0.16 wt% in kaolinite (Table 1).

Table 1. Micro chemical composition of minerals identified in the rock and weathering material as determined by EMPA analyses. Analyses are given in wt%

Mineral name	Uraninite	U-zircon	U-zircon	U-monazite	Uraninite	zircon	zircon	zircon	U-chlorite	Chlorite	Chlorite	Albite	K-feld spar	Feox
Na_2O	0.04	0.18	-0.03	0.12	1.268	0.37	0.26	0.01	0.18	0.26	0.36	11.52	0.59	0.18
MgO	0.02	-0.01	0.03	0.05	0.05	-0.01	0.01	-0.01	0.85	1.35	2.16	0.01	-0.01	0.11
Al_2O_3	0.01	0.04	0.02	0.6	0.58	0.11	0.19	0.14	3.65	5.1	6.84	19.72	19.03	0.32
SiO_2	0.42	30.18	30.01	1.55	1.31	30.61	30.34	30.89	31.90	33.81	43.89	69.37	62.11	6.04
K_2O	-0.24	-0.01	-0.01	0.14	-0.44	-0.01	0.03	0.01	0.37	0.83	0.64	0.21	14.65	0.01
CaO	0.16	0.03	0.04	1.53	2.16	1.23	1.23	1.05	22.55	28.64	30.79	0.28	0.17	78.62
FeO	0.29	0.25	0.71	1.01	0.59	0.69	0.86	0.51	0.63	0.57	0.82	0.05	-0.05	0.02
PbO	9.52	0.26	0.18	-0.29	8.81	0.59	0.29	-0.11	0.12	0	0.29	-0.17	0.06	0.72
ThO_2	20.09	-0.03	0.05	0.46	2.12	0.17	0.09	0.12	22.50	7.43	0.13	-0.03	-0.09	0.08
UO_2	58.48	0.12	0.27	0.67	80.83	0.72	0.74	0.44	2.25	0.35	0.07	-0.09	-0.08	-0.19
SO_2	0.08	0.02	0.21	-0.05	0.04	-0.02	-0.02	0.13	-0.09	-0.11	0.38	0.06	-0.04	0.39
ZrO_2	0.62	60.67	63.2	-0.89	0.11	59.3	57.49	61.55	0.08	0	0.09	0.10	-0.05	0.13
La_2O_3	-0.07	0.23	-0.17	14.33	-0.17	-0.03	0.23	-0.08	0.03	0.33	0.31	-0.27	-0.21	0.19
TiO_2	0.21	-0.15	-0.11	0.08	0.15	0.14	0.06	-0.06	0.10	0.14	0.11	-0.11	0.13	0.02
MnO	0.02	0.07	0.02	-0.44	0.15	0.06	0.03	0.03						
Nd_2O_3	1.66	0.32	-0.13	11.13	0.13	-0.47	-0.13	0						
Ce_2O_3	0.85	0.27	-0.11	24.60	-0.04	0.02	-0.05	0.14	0.66	0.48	0.44	0.07	0.31	0.2
Y_2O_3	0.71	0	0.03	2.59	1.01	0.19	0.38	0.19						
P_2O_5	0.11	0.14	-0.2	24.61	-0.02	-0.06	0	0	1.15	0.49	0.17	-0.07	-0.02	0.09
Total	93.3	92.78	94.77	83.54	99.33	94.23	92.29	95.23	87.07	79.79	87.52	101.41	97.07	87.17

Mineral name	Saprolite							Horizon B					
	U- monazite	U-Florencite	Apatite	K-Flp	Epidote	U-monazite	Uranothorite	Kaolinite +FeOx	U-Rhabdophane	Uranothorite	Kaolinite	U-zircon	Kaolinite
Na_2O	0.28	0.22	0.02	0.46	0.01	0.14	0.28	0.14	0.01	0.17	0.17	-0.15	0.06
MgO	0.02	-0.01	-0.06	0.03	0.07	0.05	-0.01	0.27	0	-0.004	0.08	0.04	0.73
Al_2O_3	3.78	28.87	0.08	18.92	18.56	0.57	0.03	32.99	8.31	0.01	15.10	0.47	25.61
SiO_2	0.21	0.11	0.28	63.13	34.97	0.17	19.42	38.77	11.10	18.43	30.07	34.7	33.97
K_2O	0.01	0.13	0.03	15.05	0.12	0.015	-0.18	0.65	0.08	-0.18	0.29	0.19	0.18
CaO	2.91	2.20	56.17	0.05	10.35	1.65	3.83	0.33	1.73	3.62	0.55	0.41	0.34
FeO	0.82	1.88	0.08	0.14	14.24	0.89	0.12	9.48	2.97	0.12	27.27	0.91	26.48
PbO	1.84	-0.17	0	-0.03	0.77	4.95	0.48	0.21	-0.73	0.47	0.07	0.18	0.17
ThO_2	0.08	0.06	-0.19	-0.08	1.73	0.17	42.83	0.12	1.68	40.83	1.16	0.24	1.21
UO_2	0.28	0.16	-0.07	0.13	-0.25	1.94	26.36	0.16	0.21	24.37	0.15	0.40	0.14
SO_2	2.82	0.71	0.15	0.02	0.42	0.35	-0.03	0.09	-0.16	-0.03	0.24	0.01	0.14
ZrO_2	-0.67	-0.83	0	0.05	0.69	0	0.67	0.15	-0.90	0.67	-0.14	56.03	0.28
La_2O_3	12.28	4.10	0.16	-0.03	0.42	17.46	0.16	0.15	20.30	0.06	-0.17	-0.08	-0.12
TiO_2	0.05	-0.04	0	-0.03	0.48	0.03	0.10	0.85	0.24	0.10	1.12	-0.02	0.16
MnO	-0.25	-0.08	-0.12	0	0.18	-0.21	0.05	0.06	-0.20	0.05	0.07	0.05	-0.03
Nd_2O_3	8.31	1.17	0.14	0.07	0.68	7.45	0.37	-0.07	8.85	0.27	-0.03	-0.09	-0.17
Ce_2O_3	22.49	8.42	-0.14	1.02	0.48	26.62	-0.07	-0.35	2.38	-0.07	-0.22	0.08	0.19
Y_2O_3	2.38	0.47	0.08	-0.04	-0.27	1.85	0.08	0	5.02	0.08	0.20	0.17	0.07
P_2O_5	24.23	26.82	39.46	0.15	1.83	29.09	0.22	1.22	24.78	0.22	2.17	0.10	1.30
Total	82.83	75.33	96.64	99.21	86.01	93.41	95.03	85.51	87.70	91.03	78.59	94.02	90.93

Table 2. Major, trace and REE composition of the rock and weathering material. The major elements are given in wt% while the trace and REEs are given in ppm

Type			Ngombas weathering material							
	Parent rock		saprolite					Horizon B		Horizon Ah
Color	Greenish		Yellow					Red		Black
Sample	NG1	NG2	NG3	NG4	NG5	NG6	NG7	NG8	NG9	NG10
SiO_2	61.1	60.3	58.2	56.3	61.6	62.1	58.1	54.7	57.7	57.6
TiO_2	0.49	0.55	0.58	0.72	0.29	0.18	0.59	1	0.98	0.9
Al_2O_3	17.25	16.75	19.35	17.4	19.75	19.95	19.15	20.8	20	18
Fe_2O_3	4.83	5.15	4.92	8.52	3.57	2.23	4.98	6.08	5.13	4.38
MnO	0.12	0.15	0.04	0.1	0.03	0.01	0.02	0.03	0.02	0.04
MgO	0.51	0.6	0.12	0.47	0.16	0.13	0.13	0.14	0.11	0.09
Na_2O	3.51	5.59	2.17	2.69	2.8	2.78	2.97	0.39	0.4	0.42
CaO	2.28	2.82	0.54	2.03	0.23	0.19	0.34	0.07	0.05	0.12
K_2O	8.57	6.12	9.74	7.85	9.7	10.05	8.77	7.2	8.36	9.34
P_2O_5	0.13	0.65	0.14	0.11	0.08	0.06	0.14	0.14	0.13	0.13
LOI	0.48	0.44	2.36	3.01	2.83	2.51	3.12	9.46	7.87	9.52
Total	101.27	98.4	100.19	100.97	101.86	101.06	99.28	100.69	101.62	101.45
SiO_2/Al_2O_3	3.54	3.00	3.01	3.24	3.12	3.11	3.03	2.63	2.89	3.20
CIA	54.57	59.23	60.85	58.06	60.81	60.51	61.32	73.09	69.42	64.56
ppm										
Ba	10000	1425	10000	10000	6220	6650	6530	5450	6290	6980
Cr	10	50	10	10	10	10	10	170	600	210
Cs	6.6	1.47	7.05	6.27	1.67	1.41	0.91	3.61	3.51	3.34
Ga	27.6	22.5	30.5	30.4	22.8	22.1	26.1	29.1	26.9	23.7
Nb	106.5	42.1	136.5	106	16.4	7.9	54.8	55.2	58	66.9
Rb	339	95.6	379	314	227	238	172.5	219	250	273
Sn	3	2	2	3	1	1	2	3	2	2
Sr	6120	1770	5650	4120	1330	1345	2480	833	879	980
Ta	3.5	2.5	4.7	4.5	1	0.5	3.2	3	3.1	3.3
V	70	107	74	135	38	24	60	94	85	69
Y	82.8	28.8	27.6	39.9	14.8	7.5	7.4	11.3	9.8	10
Zr	1830	941	2660	2250	218	93	1060	1430	1420	1760
Co	3	27	4	4	4	4	3	5	4	5
Cu	23	816	26	17	27	29	31	24	18	20
Li	10	10	10	10	10	10	10	10	10	10
Mo	6	7	2	3	3	2	3	9	8	7
Ni	11	62	7	8	10	8	8	19	16	13
Sc	1	5	1	3	4	4	3	7	5	4
Hf	29.7	20.1	42.6	38.8	4.9	2.2	17.3	25.4	25.7	30.7
Tl	10	10	10	10	10	10	10	10	10	10
Zn	89	93	38	121	48	38	70	71	32	36
Pb	145	47	153	156	17	14	24	44	40	45
U	50.6	12.35	66.9	52.7	16.25	16.25	9.22	11.95	11.1	12.8
Th	215	192	284	337	17.2	7.52	60.7	56.2	51.2	59.7
Th/U	4.25	15.55	4.25	6.39	1.06	0.46	6.58	4.70	4.61	4.66
Pb/U	2.87	3.81	2.29	2.96	1.05	0.86	2.60	3.68	3.60	3.52
ppm										
La	313	197.5	162	132.5	85.9	45.3	45.8	86.4	77	68.6
Ce	608	318	300	289	179.5	94.9	105.5	173	137	124
Pr	64.4	34.1	31.7	28.7	19.8	10.35	12.55	17.4	15.45	13.7
Nd	227	117.5	107	101	71.7	38	42.7	59.9	53.3	47.8
Sm	35.6	18.35	15.55	17.9	10.85	5.56	6.69	8.72	8.03	6.93
Eu	10.45	5.13	4.48	5.48	2.81	1.51	2.05	2.15	1.86	1.77
Gd	24.5	11.7	9.41	11.7	6.27	3.22	3.38	5	4.48	3.89
Tb	3.44	1.28	1.26	1.66	0.82	0.4	0.49	0.69	0.54	0.58
Dy	16.45	5.61	5.84	8.34	3.24	1.72	2.08	3.19	2.43	2.44
Ho	3.09	0.94	1.07	1.46	0.58	0.3	0.37	0.53	0.48	0.45
Er	7.62	2.49	2.82	4.03	1.17	0.71	0.86	1.25	1.21	1.1
Tm	1.02	0.31	0.39	0.57	0.16	0.05	0.14	0.17	0.12	0.12
Yb	5.77	1.9	2.44	4.06	1.02	0.54	0.76	1.29	1.03	1.11
Lu	0.73	0.29	0.35	0.56	0.13	0.09	0.12	0.18	0.15	0.16
∑REE	1321.07	715.1	644.31	606.96	383.95	202.65	223.49	359.87	303.08	272.65
(La/Yb)N	36.85	70.61	27.11	22.17	57.21	56.99	40.94	45.50	50.78	41.98
Ce/Ce* (1)	1.04	0.94								
Eu/Eu* (1)	1.08	1.07								
Ce/Ce* (2)			0.98	1.09	1.02	1.02	1.03	1.04	0.93	0.94
Eu/Eu* (2)			1.05	1.07	0.96	1.01	1.22	0.92	0.88	0.96

4.3. Geochemistry of Syenite and Weathering Materials

4.3.1. Syenite Geochemistry

The major, trace and REE composition of the syenite and the weathering materials are given in Table 2. Syenite is enriched in SiO_2 (average 60.7 wt%). It shows moderate alkali contents (K_2O averages 7.34 wt%, Na_2O averages 4.55 wt% with an average of 2.55 wt% for CaO). The CIA and LOI values in syenite are 54.57 and 0.48 respectively. Syenite reveals moderate to high concentrations of fluid-immobile elements such as Al (averages 17 wt% Al_2O_3), Zr (1385.5 ppm Zr), Th (203.5 ppm Th), Y (55.8 ppm Y) and Hf (24.9 ppm Hf). U content reaches a high of 50.6 ppm, coupled with elevated concentration of Ba, Sr, Nb, Rb and Pb (Table 2).

4.3.2. Geochemistry of Weathering Materials

High content of SiO_2 (average 59.26 wt%) and moderate concentrations of alkali elements (K_2O average 9.22 wt% and Na_2O average 2.69 wt%) are observed in saprolite. The CIA and LOI values are 60.31 and 2.76 respectively. The concentrations of fluid-immobile elements such as Al (average 19.12 wt% Al_2O_3), Zr (average 1256.2 ppm Zr), Th (average 141.2 ppm Th), Y (average 19.44 ppm Y) and Hf (average 21.16 ppm Hf) are moderate to high in saprolite. The concentration of U in the saprolite horizon reaches a maximum of 66.9 ppm. This is coupled with elevated contents of Ba, Sr, Nb, Rb and Pb (Table 2).

The B horizon shows high contents of SiO_2 (average 56.2 wt%) and moderate contents of the alkalis (K_2O with an average 7.78 %). CIA value shows an average of 71.26 and a LOI which averages 8.67. It is characterized by moderate to high concentrations of fluid-immobile elements such as Al (average 20.4 wt% Al_2O_3), Zr (average 1425 ppm Zr), Th (average 53.7 ppm Th), Y (average 10.55 ppm Y) and Hf (average 25.55 ppm Hf). The concentration of U averages 11.53 ppm. This is coupled with elevated contents of Ba, Sr, Nb, Rb, Zn, Cr and Pb (Table 2).

The Ah horizon shows high SiO_2 content (average 57.6 wt%), moderate alkali concentration (K_2O average 8.3 wt% and Na_2O average 0.4 wt%). CIA and LOI are respectively 64.56 and 9.52. Fluid-immobile elements show high concentration examples Al (18 wt% Al_2O_3), Zr (1760 ppm Zr), Th (59.7 ppm Th), Y (10 ppm Y) and Hf (30.7 ppm Hf). The concentration of U in this horizon reaches a maximum of 12.8 ppm, coupled elevated concentrations of Ba, Sr, Nb, Rb, Zn, Cr and Pb (Table 2).

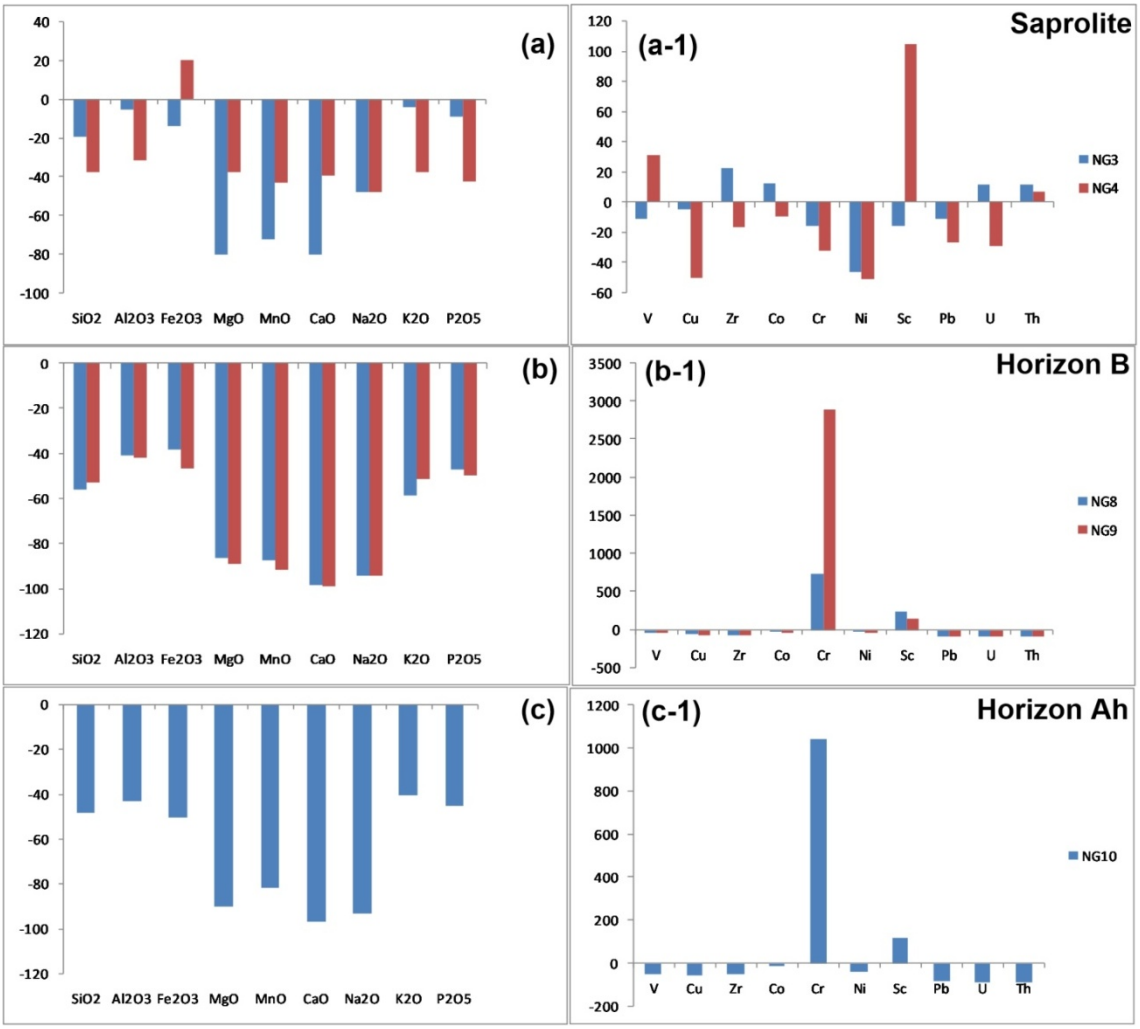

Figure 6. Histograms showing the gain/loss of major oxides and trace elements in the the weathering materials developed on syenite in the Ngombas area. Calculations are based on the immobile element method with TiO_2 as the least mobile element and the average composition of the fresh syenite used as the unaltered reference protolith. a, b and c represent the major elements data for the alteration categories while a-1, b-1 and c-1 represent the trace elements counterparts

4.4. Element Mobility during Weathering as Determined by Mass Balance

Gain and loss diagrams were constructed (Figure 6) to depict the element mobility from syenite to the weathering blanket. The weathering materials show depletions in SiO_2, Al_2O_3, MnO, MgO, Na_2O, CaO, K_2O and P_2O_5 excepted of Fe_2O_3 which shows an enrichment in the saprolite horizon NG4.

Several elements are depleted from the sprolite, B and Ah horizons, with the exception of V, Zr, Co, Sc, U and Th which shows enrichments in samples NG3 and NG4 from the saprolite horizon respectively (Figure 6a and Figure 6a-1). In the B horizon, major elements are lost while trace elements such as Cr and Sc are gained (Figure 6b and Figure 6b-1). The Ah horizon shows depletion in the major element, this is coupled with and enrichment in Cr and (Figure 6c and Figure 6c-1).

5. Discussion

5.1. Regolith Developed on Syenite

The Weathering profile developed on the syenite reveal three horizons from bottom to top: they include the saprolite, B and Ah horizons. Relics of primary minerals identified are plagioclase, amphibole and quartz (Figure 3e and Figure 3f).

The increase of loss element (U, Th, Fe_2O_3, MgO, Na_2O, CaO) observed on the figure of gain and loss justify the degree of weathering of blanket. The B and Ah horizons show the absence of minerals such as amphibole, biotite and pyroxene (Figure 3f). The disappearance of texture from the saprolite to the Ah horizon indicates the increase of weathering rate in the profile. The disappearance of texture from the saprolite to the Ah horizon indicates an increase in the rate of weathering in the weathering profiles. Especially in horizons B and Ah, the relics of primary minerals are surrounded in clayey matrix.

The clay minerals identified in these horizons include chlorite, vermiculite and kaolinite (Figure 5c and Figure 5d).

The abundance of kaolinite in horizon B and Ah shows that the monosialitization processes predominate bisialitization according to [27]. The abundance of goethite in the Ah horizon comparatively to saprolite and B horizon attest to increase in meteoritic alteration from the bottom to the top (Figure 5a). The increase of goethite and the clays minerals from saprolite to horizon B attest an increasing the degree of weathering and the effect of meteoric alteration.

5.2. U-bearing Mineral Phases

Uraninite is the main uranium phase identified in syenite. EMPA analyses of uraninite indicate the presence of thorium (Table 1). This is similar to uraninite reported in granites albitites from the uraniferous province in Ukraine [54]. Impurities in uraninite suggest the coexistence between uranium and thorium in the melt source. The presence of U, Zr and Y in thorite suggests a solid solution which is the case with the thorite from the Ngombas area [55] showed that the presence of U, Zr and Y in thorite suggests the presence of solid solution such as the case with the thorite from the Ngombas area. Uraninite occurs as inclusions in zircon. Inclusion of U-oxide in zircon indicates a magmatic process. Studies of [25,26,56] reported similar cases of uraninite in primary minerals (quartz, k-feldspar) in granite. This magmatic origin is also supported by the presence of accessory minerals in the syenite such as U-monazite and U-xenotime.

5.3. Uranium Mobilization and Retention in the Regolith

We have shown that the regolith indicates the absences of uraninite. The formation of new U mineral phases in the regolith depends on the oxidizing condition, secondary minerals and phosphates in the weathering blanket. Oxidizing condition induce high dissolution of uraninite and their migration as uranyl (UO_2^+) [57]. In the weathering blanket, uranyl is sorbed and/or sequestrated by various mineral phases [20]. The saprolite horizon shows uranothorite bearer on chlorite. These minerals suggest the sorption of uranyl on thorite mineral which one is considered as refractory mineral. The sorption process of uranyl reduces the mobility of uranium [58,59,60]. U-monazite is the only primary mineral that bears U in the regolith. Their resistant to weathering [61] prevents further migration of uranium. Due to mechanical and chemical weathering, these accessories minerals are generally associated with clay minerals of the weathered products and contribute to the stabilization of uranium in the regolith. Phosphates enhance the adsorption of U in the regolith and contribute to the formation of new uranium phases [62]. Thus, the U-florencite ($CeAl_3(PO_4)_2(OH)_6$) aids in the reduction of U mobility and facilitate the retention of uranium in the regolith in Ngombas.

In the B horizon, the presences of uranothorite attest to the resistance of this uranium mineral and play an important role in the mobility and retention of uranium in Ngombas profile. In this horizon, zircon identified bears uranium. Zircon is a resistant mineral during weathering process [61] Just like the monazite in saprolite horizon, zircon contributes to the stabilization of uranium in this horizon [20]. Phosphate minerals such as apatite, monazite and other primary phosphates participate to the sequestration process of uranium [20,21,22]. EMPA analyses reveals as high as 0.21 wt% of U in rabdophane (Ce, La (PO_4) (H_2O)) (Table 2). U sorption in clay minerals could be tied to high cationic capacity and organized crystalline pattern [19]. Fe-oxides and clay minerals play an important role in actinides migration such as radionucleides, trapping uranyl as inner- and/or outer-sphere complexes at their surface [20,25,64,65]. This sorption is more evidence in clay mineral blends with high Fe-oxides contents [64]. The weathering blanket reveals as high as 0.15wt% U in kaolinite. The concentration of U becomes higher as kaolinite blends with Fe-oxides (0.15 wt%). Thus the retention of U in this horizon is attributed to the presence of clay minerals.

In horizon Ah, the absence of new uranium phases suggests that oxidizing condition induce the solubility of previous U phases [22,23]. Nevertheless, the presence of

organic matter in this horizon suggests the U was sorbed as nanocrystals of uraninite in organic matter [66].

5.4. Environmental Impact of U Mobilitization

U migration in waste rock and/or in natural soils depends on oxidizing condition, pH and U-speciation [20,64,66]. Generally, U is mobilized as uranyl and/or uranyl phosphate in groundwater or associated in particles in the environment [26,69]. The source of U in Ngombas profile is attributed to dissolution of uraninite inclusion in zircon. The other U-bearing mineral present is monazite, which is considered as accessory mineral and resists to meteoritic weathering [61]. The weak weathering rate of zircon and monazite could explain the feeble content of uranium in the horizon. Nevertheless it could suggest another source not identified in this study.

The presence in soil profile of uranothorite shows that uranyl mobilized is sorbed on thorium mineral and contribute to reduce the impact of uranium in the environment. Reference [20] reported that phosphate minerals such as apatite, monazite and other primary phosphates play the important role in U sequestration. U-florencite and U-rhabdophane present in the Ngombas profile attest that the phosphates minerals sequestrated U-dissolved and limiting the mobility of (UO_2^{2+}) in the subsurface environment. References [18,19,70] reported that clay minerals and Fe-oxides contribute to reduce the impact of uranium in the environment by their sorption capacity. As the previous research, the presence of uranium content in kaolinite and the increasing of this content in Fe-oxides blend kaolinite show the impact of clays and oxides in the migration of uranium in the Ngombas environment. Also, the presence of phosphate and vegetation could promote the formation of (nanocrystal) uranyl phosphates, thereby limiting the migration of uranyl in Ngombas surface environments [59].

6. Conclusion

The soil profile of Ngombas is developed on the syenite. Three horizons are distinguished from the bottom to the top: saprolite, B and Ah horizons. The syenite is composed of plagioclase, potassic feldspar, amphibole, pyroxene, biotite, quartz, hematite and zircon. The horizons show relics of plagioclase, amphibole, quartz, hematite and goethite. Clay minerals are more abundant from the top to the bottom of profile and include: chlorite, vermiculite and kaolinite. The intensity of weathering increase from the bedrock to the Ah horizon. CIA values vary from 56.9 to 71.26 % respectively from the syenite to Ah horizon. Also, gain and loss of chemical elements show the decreasing of major elements from saprolite to Ah horizon.

EMPA analyses show the uraninite in zircon inclusion in the syenite. U-monazite and U-zircon are the accessories minerals bearing uranium in the rock. Uraninite is not identified in saprolite, uranothorite is a new phase presents in the horizons. It is associated to U-zircon and U-monazite with the new phospahte mineral U-florencite and U-rhabdophane. That minerals and Fe-oxides blended kaolinite in soil profile contribute to limit the mobility of uranium in the Ngombas environment.

Acknowledgements

The authors wish to acknowledge funding from IMPMC (Institut de Minéralogie et de Physique des Matériaux et de Cosmochimie) that covered the research stay of JSM at the Institut de Minéralogie, de Physique des Matériaux et de Cosmochimie in France. They also thank the engineers of the OCEAN Department of IRD, Bondy France, T. Pilorge, S. Caquineau, for their technical assistance and advice.

References

[1] Nahon, D,. *Evolution of iron crusts in tropical landscapes.* In:Coleman, S.M., Dethier, D.P. (Eds.), Rates of chemical weathering of rocks and minerals. Academic Press, pp. 169-191. 1986.

[2] Kamgang Beyala V., Ekodeck G. E., *Altération et bilans géochimiques des biotites des gneiss de Nkolbisson (NW de Yaoundé, Cameroun).* Géodynamique 6 (2), 191-199. 1991.

[3] Tardy, Y. *Petrology of laterites and tropical soils.* A.A. Balkema, Rotterdam, The Netherlands, Brookfield, VT, USA. 1997.

[4] Traoré D., Beauvais A., Augé T., Chabeaux F., Parisot J. C., Cathelineau M., Peiffort C., Colin F. *Platinum and palladium mobility in supergene environment: the residual origin of the pirogues river mineralization.* New Caledonia Journal Geochemical Exploration 88, 350-354. 2006.

[5] Etame, J., Suh, C.E., Gerard, M., Bilong, P., *Phillipsite formation in nephelinitic rocks in response to hydrothermal alteration at Mount Etinde, Cameroon.* Chemie der Erde-Geochemistry 72, 31-37. 2012.

[6] Leprun J. C. *Ferugineous cuirasses of crystalline countries of dry western Africa*. Genesis-Transformation-Degradation. Doctorate thesis ès Sciences Géologie. P. 224. 1979.

[7] Bocquier G., Muller J. P., Boulangé B. *Laterites: current knowledge and perspectives on their differentiation mechanisms.* Sci. Soil, fiftieth jubilee book of IAFES, pp. 123-138. 1984.

[8] Bilong p., Eno Belinga S. M., volkoff B. *Séquence d'évolution des paysages cuirassés et des sols ferrallitiques en zones forestières tropicales d'Afrique centrale. Place des sols à horizon d'argile tachetée.* Comptes rendus académies sciences. Paris, série. 11. 1992.

[9] Oliveira T. S., Fontes M. P. F., Da Costa L. M., Horn A. H. *Relationship between magnetization and trace element content of Brazilian soils from different parent materials*. Soils Sciences. 165 (10): 825-834. 2000.

[10] Temgoua E., Hans-Rudolf P., Bitom D. *Trace element differentiation in ferruginous accumulation soil patterns under tropical rainforest of southern Cameroon, the role of climatic change*. The Science of the Total Environment. 303. 203-214. 2003.

[11] Braun, J.-J., Ndam Ngoupayou, J.R., Viers, J., Dupre, B., Bedimo Bedimo, J.-P., Boeglin, J.-L., Robain, H., Nyeck, B., Freydier, R., Sigha Nkamdjou, L., Rouiller, J., Muller, J.-P., *Present weathering rates in a humid tropical watershed: Nsimi, South Cameroon*. Geochimica et Cosmochimica Acta 69, 357-387. 2005.

[12] Ebah A. S., Ndigui P. D., Beyanu A. A., Teutsong T., Bilong P. *Geochemistry of pyroxenites, amphibolites and their weathered products in the Nyong unit, SW Cameroon (NW border of Congo craton): Implication for Au-PGE exploration*. Journal of Geochemical Exploration. 114: 1-19.

[13] Ndjigui, P.-D., Bilong, P., Bitom, D., Dia, A., *Mobilization and redistribution of major and trace elements in two weathering profiles developed on serpentinite in the Lomié ultramafic complex, South-East Cameroon*. Journal of African Earth Sciences 50, 305-328. 2008.

[14] Ndjigui P. D., Badinane M. F. B., Nyeck B., Nandjip H. P. K., Bilong P. *Mineralogy and geochemical features of the coarse*

saprolite developed in the SW of Yaoundé, South Cameroon. Journal of African Earth Sciences. 79, 125-142. 2013.

[15] Leybourne, M.I., Goodfellow, W.D., Bowle, D.R., Hall, G.M., *Rapid development of negative Ce anomalies in surface waters and contrasting REE patterns in ground waters associated with Zn-Pb massive sulphide deposits.* Applied Geochemistry 15, 695-793. 2000.

[16] Borovec, Z. *The adsorption of uranyl species by fine clay.* Chemical Geology, 32 45-58. 1981.

[17] Sylwester E.R., Hudson, E.A., Allen, P.G. *The structure of uranium (VI) sorption complexes on silica, alumina, and montmorillonite.* Geochim. Cosmochim. Acta 64, 2431-2438. 2000a.

[18] Catalano, J.G., Brown Jr., G.E. *Uranyl adsorption onto montmorillonite: evolution of binding sites and carbonate complexation*. Geochemical Cosmochimical. Acta 69, 2995-3005. 2005.

[19] Campos, B., Aguilar-Carrillo, J., Algarra, M., Gonçalves, M. A., Rodríguez-Castellón, E., Joaquim, C.G. Esteves da Silva, Bobos, I. *Adsorption of uranyl ions on kaolinite, montmorillonite, humic acid and composite clay material*. Applied Clay Science 85. 53-63 Elsevier. 2013.

[20] Kanzari, A., Gérard, M., Boekhout, F., Galoisy, L., Calas, G., Descostes, M. *Impact of incipient weathering on uranium migration in granitic waste rock piles from former U mines (Limousin, France).* Journal of Geochemical Exploration. 183, 114-126. 2017.

[21] Jerden, Jr J.L., Sinha, A. K, Zelazny, L.. *Natural immobilization of uranium by phosphate mineralization in an oxidizing saprolitesoil profile: chemical weathering of the Colles Hill uranium deposit, Virginia.* Chemical Geology, 199: 129-57. 2003.

[22] Jerden, Jr., Sinh, A. K. *Geochemical coupling of uranium and phosphorous in soils overlying an unmined uranium deposit: Coles Hill, Virginia*. Journal of Geochemical Exploration 91, 56-70. 2006.

[23] Langmuir, D., Herman, J. S. *The mobility of thorium in natural waters at low temperatures.* Geochemical of Cosmochimical. Acta 44, 1753-1766. 1980.

[24] Regenspurg, S., Margot-Roquier, C., Harfouche, M., Froidevaux, P., Steinmann, P., Junier, P., Bernier-Latmani, R.,. *Speciation of naturally-accumulated uranium in an organic-rich soil of an alpine region (Switzerland)*. Geochimical Cosmochimical Acta 74, 2082-2098. 2010.

[25] Cabral Pinto, M.M.S., Silva, M.M.V.G., Ferreira da Silva, E, Miranda, P., Marques, R., Prudêncio, I., Rocha, F. *Uranium Contents in the Lithological Formations of Santiago Island, Cape Verde*. Earth and Planet. Sciences 8, 18-22. 2014.

[26] Boekhout, F., Gérard, M., Kanzari, A., Michel, A., Déjeant, A., Galoisy, L., Cala, G. *Uranium migration and retention during weathering of a granitic waste rock pile*. Applied Geochemistry 58, 123-135. 2015.

[27] Tsozué D., Ndjigui P. D. Geochemical Features of the Weathered Materials Developed on Gabbro in a Semi-Arid Zone, Northern Cameroon. Geosciences, 7, 16; 2017.

[28] Briqueu, L., Lancelot, J.R., Valois, J. P., Walgenwitz, F. *Geochronologie U-Pb et génèse d'un type de minéralisation uranifère: les alaskites de Goanikontes (Namibia) et leur encaissant.* Bulletin Centrale De Recherche Exploration-Production, Elf Aquitaine 4, 759-811. 1980.

[29] Bowden, P., Herd, D., Kinnaird, J.A. *The significance of Uranium and Thorium concentrations in pegmatitic leucogranites (alaskites), Rossing Mine, Swakopmund, Namibia*. Communications of the Geological Survey of Namibia 10, 43-49. 1995.

[30] Parnell J. *Petrographic relationships between mineral phases and bitumen in the Oklo Proterozoic natural fission reactors, Gabon*. Mineralogical Magazine, 60, 581-593. 1996.

[31] Herd, D.A., *Geochemistry and mineralization of alaskite in selected areas of the Reossing Uranium Mine, Namibia*. M.Sc. Thesis (Unpubl.), University of St. Andrews, Scotland. P. 205. 1997.

[32] Basson, I.J. *Fault modeling in the Rossing Uranium Mine, Namibia*. Report for Moore, Spence and Jones and Rio Tinto, 44 pp. 2001a.

[33] Nex, P.A.M., Kinnaird, J.A., Oliver, G. J. H. *Petrology, geochemistry and mineralization of post-collisional magmatism in the southern Central Zone, Damaran Orogen, Namibia*. Journal of African Earth Sciences 33, 481-502. 2001a.

[34] Basson, I.J., Greenway, G. *The Rossing Uranium Deposit: a product of late-kinematic localization of uraniferous granites in the Central Zone of the Damara Orogen, Namibia.* Journal of African Earth Sciences 38. 413-435. 2004.

[35] Kouske, A. P., Suh, C.E., Ghogomu, R. T., Ngako, V. *Na-Metasomatism and Uranium Mineralization during a Two-Stage Albitizationat Kitongo, Northern Cameroon: Structural and Geochemical Evidence*. International Journal of Geosciences 3, 258-279. 2012.

[36] Mosoh Bambi, C.K, Suh, C.E., Nzenti, J.P., Frimmel, H.E. *U-Mo mineralization potential in Pan-African granites, southwestern Cameroon: Economic geology of the Ekomédion prospect.* Journal of African Earth Sciences 65, 25-45. 2012.

[37] Embui V. F., Suh C. E., Cottle J. M., Etame J., Mendes J., Agyingi C. M., Vishiti A., Shemang E. M., Lehmann B. Zircon chemistry and new laser ablation U-Pb ages for uraniferous granitoids in SW Cameroon. Acta Geochimical. 2019.

[38] Bute, S. I., Yang, X., Suh, C. E., Girei, M. B., Usman, M. B. *Mineralogy, geochemistry and ore genesis of Kanawa uranium mineralization, Hawal Massif, eastern Nigeria terrane: Implications for uranium prospecting in Nigeria and Cameroon.* Ore Geology Reviews (2020).

[39] Kouske, A. P. *Uranium occurrences associated with sodium metasomatism within the Pan-African mobile zone- the Kitongo, Salaki and Mayo Nielse uranium mineralizations in the Poli region, northern Cameroon: petrographic, geochemical and structural investigations*. University of Yaounde I. PhD thesis. PP 264. 2013.

[40] Maurizot, P. Abessolo, A. Feybesse, J.L., Johan Lecomte P. *Etude de prospection minière du Sud-Ouest Cameroun*. Synthèse des travaux de 1978 à 1985. Rapport de BRGM 85: 274p. 1986.

[41] Ele, A.P., Owono, A.P., Ekobena, F.H., Ben-Bolie, G.H., El Khoukhi, T. *High background radiation investigated by gamma spectrometry of the soil in the southwestern region of Cameroon.* J. Environ. Radioact. 101, 739-743. 2010.

[42] Mvondo S., Ben-Bolie G.H., Ema'a Ema'a J.M., Owono Ateba P., Ele abiama P., Beyala Ateba J.F. *Study of soil-fern transfer of naturally occurring alpha emitting radionuclides in the Southern Region of Cameroon*. Journal of Environmental Radioactivity 180. 114-119. 2017.

[43] Braun J. J., Pagel M., Muller J. P., Bilong P., Mkhard A., Guillet B. *Cerium anomalies in lateritic profiles.* Geochimica. Cosmochimica. Acta 54, 781-795. 1990.

[44] Braun, J.-J., Pagel, M., Herbillon, A., Rosin, C. *Mobilization and redistribution of REEs and Th in syenitic lateritic profile: a mass-balance study.* Geochimica et Cosmochimica Acta 57, 4419-4434. 1993.

[45] Prian, J.P., Coste, B., Eko N'dong, J., Johan, V., Ledru, P. *Synthèse géologique et géochimique, potentialités minières du degre´carre´Boue´(Gabon central) avec carte géologique au 1/200,000.* République gabonaise. Ministère des Mines et des Hydrocarbures, Libreville, BRGM, Orléans, 103 p. 1990.

[46] Toteu, S.F., Van Schmus, W.R., Penaye, J., Nyobe, J.B. *U-Pb and Sm-Nd evidence for eburnian and panafrican high grade metamorphism in cratonic rocks of southern Cameroon*. Precambrian Research, 67, 321-347. 1994.

[47] Feybesse, J.L., Johan, V., Triboulet, C., Guerrot, C., Mayaga-Minkolo, F., Boucho, V., Eko N'dong, J. *The West Central African belt: a model of 2.5-2.0 Ma accretion and two-phase orogenic evolution.* Precambrian Research 87, 161-216. 1998.

[48] Penaye, J. Toteu, S.F. Tchameni, R. Van Schmus, W.R. Tchakounté, J. Ganwa, A.A. Minyem, D. Nsifa, E.N. *The 2.1 Ma West Central African Belt in Cameroon: extension and evolution*. Journal of African Earth Sciences 39: 159-164. 2004.

[49] Lerouge, C. Coherie A. Toteu S.F. Pénaye, J. Milesi, J.P. Tchameni, R. Nsifa, N.E. Fanny, M.C., Deloule, E. *Shrimp U-Pb zircon age evidence for Paleoproterozoic sedimentation and 2.05 Ga syntectonic plutonism in the Nyong Group, south-western Cameroon: conse-quences for the Eburnean-Transamazonian belt of NE Brazil and Central Africa*. Journal of African Earth Sciences 44 (4-5): 413-427. 2006.

[50] Messi Ottou E. J., Owona S., Mvondo Owono F., Ntomba S. M., Akame J. M., Koum S., Mvondo Ondoa J. *Analyse morphotectonique par couplage d'un modèle numérique de terrain (MNT) et des données de terrain d'une portion de zone mobile*

paléoprotérozoïque de la région de Lolodorf (Complexe du Nyong, SW Cameroun). Sciences, Technologies et Développement, 15, 24-39. 2013.

[51] Nedelec A, Minyem D, Barbey P. *High PHigh T anatexis of Archaean Tonalitic grey gneisses: the Esekamigmatites, Cameroon*, Precamb Research, 62, 191-205. 1993.

[52] Omoko M. *Dynamique de l'eau dans un sol et étude comparée entre l'évaporation mesurée et calculée en climat équatorial*. Thèse Doctorat Spéciale Université de Bordeaux. P. 59. 1984.

[53] Letouzey, R. *Notice explicative de la carte phytogéographique du Cameroun à l'échelle de 1/500000*. Institut de la carte internationale de la végétation Toulouse. 240p. 1985.

[54] Nesbitt, H.W., Young, G.M. *Early proterozoic climates and plate motions in ferred from major element chemistry lutites*, nature 299, 715-717. 1982.

[55] Cuney M., Emetz A., Mercadier J., Mykchaylov V., Shunko V., YuslenkoA. *Uranium deposits associated with Na-metasomatisme from central Ukraine: A review of some of the major deposits and genetic constraints.* Elsevier Ore Geology Reviews 44, 82-106. 2012.

[56] Forster, H.-J. *Composition and origin of intermediate solid solutions in the system thorite xenotime-zircon-coffinite*. Lithos 88 35-55. 2006.

[57] Cabral Pinto M. M. S., Silva M. M. V. G., Neiva Fernanda Guimar A. M. R., Silva P. B.,. Release, Migration, Sorption, and (Re) Precipitation of U during Peraluminous Granite Alteration under Oxidizing Conditions in Central Portugal. Geosciences, 8, 95; 2018.

[58] Grenthe, I., Drozdzynski, J., Fujino, T., Buck, E.C., Albrecht-Schmitt, T.E., Wolf, S.F., Uranium. *In: Edelstein, N.M., Fuger, J., Morss, L.R. (Eds.), The Chemistry of the Actinide and Transactinide Elements*, third ed., vol. 1. Springer, Dordrecht, pp. 253-698. Chap. 5. 2006.

[59] Duff, M. C., Coughlin, J. U. Hunter D. B. *Uranium co-precipitation with iron oxide minerals.* Geochemical et Cosmochimical Acta, 66, (20), 3533-3547. 2002.

[60] Wellman, D.W., Icenhower, J.P., Gamerdinger, A.P., Forrester, S.W. *Effects of pH, temperature, and aqueous organic material on the dissolution kinetics of meta-autunite minerals, (Na, Ca)$_2$-1[(UO$_2$)(PO$_4$)]$_2$3H$_2$O.* American Mineral. 91, 143-158. 2006.

[61] Sreejesh, N., Karimzadeh, L., Merkel, J. B. *Sorption of uranyl and arsenate on SiO$_2$, Al$_2$O$_3$, TiO$_2$ and FeOOH*. Environment Earth Sciences 72: 3507-3512. 2014.

[62] Scherrer, N.C., Engi, M., Gnos, E., Jakob, V., Lietchi, A. *Monazite Analysis; From Sample Preparation to Microprobe Age Dating and REE Quantification*. 80. 93-105. 2000.

[63] Payne, T. E., Davis, J.A., Waite, T.D. *Uranium adsorption on ferrihydrite - effects of phosphate and humic acid*. Radiochimical Acta 74 (S1), 239-244. 1996.

[64] Rowe, R. K., Quigley, R.M., Brachman, R.W.I., Booker, J.R., Brachman, R. Barrier Systems for Waste Disposal Facilities. CRC Press. ISBN 9780367863722. 2nd Edition. 2004.

[65] Brown, G.E., Calas, G. *Mineral-aqueous solution interfaces and their impact on the environment.* Geochemical Prospect. 1, 483-484. 2012.

[66] Cumberland, S.A., Douglas, G., Grice, K., Moreau, J.W. *Uranium mobility in organic matter-rich sediments: a review of geology and geochemical processes*. Earth Science Review. 159, 160-185. 2016.

[67] Neiva, A.M.R., Carvalho, P.C.S., Antunes, I.M.H.R., Silva, M.M.V.G., Santos, A.C.T., Cabral Pinto, M.M.S., Cunha, P.P. *Contaminated water, stream sediments and soils close to the abandoned Pinhal Do Souto uranium mine, Central Portugal*. Journal Geochemical Exploration 136, 102-117. 2014.

[68] Maher, K., Bargar, J.R., Brown Jr., G.E. *Environmental speciation of actinides*. Inorg. Chem. 52, 3510-3530. 2012.

[69] Brugger, J., Burns, P.C., Meisser, N. *Contribution to the mineralogy of acid drainage of uranium minerals: marecottite and the zippeite-group*. American Mineral. 88 (4), 676-685. 2003.

[70] Schlegel, M.L., Descostes, M. *Uranium uptake by hectorite and montmorillonite: a solution chemistry and polarized EXAFS study*. Environment Sciences Technology 43, 8593-8598. 2009.